Theory of laser oscillation on two or more coupled transitions*

F. Najmabadi, M. Sargent III, and F. A. Hopf
Optical Sciences Center, University of Arizona, Tucson, Arizona 85721
(Received 17 March 1975)

Aid or competition between two laser modes oscillating on different transitions of a three-level medium are studied following the method of Lamb. An arbitrary amount of Doppler broadening is allowed for. The "electric-quadrupole" term generated by back-to-back transitions of the two modes but having vanishing electric dipole moment is found to have little effect on the oscillation intensities in typically observed circumstances. This fact justifies, in part, the rate-equation approximation commonly used in multilevel analysis. For a bidirectional ring cascade configuration, however, this coherence term can be important because of constructive interference familiar from two-photon, Doppler-free spectroscopy. The ordinary (i.e., hole-burning) cross-saturation terms for cascade transitions produce mutual mode aid, rather than competition as in the competitive cases. A curious consequence of this difference is greater accuracy in the third-order theory of cascade transitions than in that of competitive transitions, as a result of partial cancellation of errors incurred through neglect of higher orders. The treatment is generalized to multilevel media (four or more levels) with numerical illustration and discussion of the method's relationship to laser oscillation involving diatomic molecules.

I. INTRODUCTION

In 1957 a theory was proposed by Javan[1] for a three-level maser oscillator. By introducing a high-intensity saturating field between two levels, he showed that an induced emission of power at a lower frequency corresponding to a transition between an intermediate energy level and one or the other of the two levels can occur. In 1963 and 1964 the detection of two- and three-step laser cascades were reported in a series of papers. A list of these papers is given in Haken, Der Agobian, and Pauthier's[2] paper of 1965, which treats a solid-state two-step cascade laser using the second-quantization formalism. For the description of many phenomena, the semiclassical Lamb theory[3] is accurate (see for example Ref. 4), and simpler than the fully quantum-mechanical treatment. Hence, most work (including the present paper) is based on a semiclassical model. The problem of laser-induced line narrowing on two coupled transitions has been studied by Feld and Javan[5] for the case of laser transitions detuned from the center of its atomic gain profile and later for a high-intensity gas laser by Feldman and Feld.[6,7] Feld and Javan,[5] by scanning the gain profile with a weak monochromatic probe field collinear with the laser field, found two sharp resonances at frequencies symmetric about the line center. One of the peaks was considerably narrower than the other, and both were much narrower than the Doppler width of the laser field. They named this effect "laser-induced line narrowing." The theory of a three-level gas-laser amplifier has been treated semiclassically by Hänsch and Toschek.[8] A good review and list of references of the work to date is given in that paper and in the review paper by Beterov and Chebotaev.[9]

In this paper we extend the theory of Lamb[3] to treat the problem of both homogeneous and Doppler-broadened three-level laser media. We treat two configurations known as cascade and competitive, which are shown in Fig. 1. In addition, we treat multilevel cascades in which a distinct mode of the field oscillates between individual level pairs. This theory is applicable to some features of diatomic molecular lasers. The choice of notation allows results obtained for the cascade case to give corresponding results for the competitive case by inspection. The remainder of this section defines notation and philosophy of our models. Further background material is given in Refs. 4 and 10.

As in the Lamb theory, each mode is assumed to be plane wave usually with sinusoidal z dependence (running-wave cases are discussed in Appendix A):

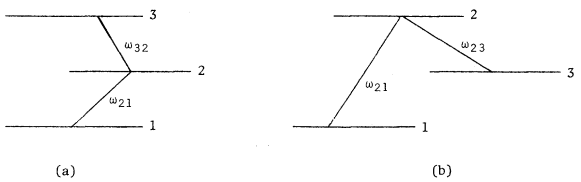

FIG. 1. Two cases of the three-level transitions. (a) Cascade case in which transitions between 3 and 2 levels and between 2 and 1 levels are allowed. (b) Competitive case with allowed transitions between 2 and 3 levels and between 2 and 1 levels. The multilevel cascade is depicted in Fig. 12. The level numbering in the competitive case is chosen to allow cascade formulas to be used (with trivial modification) for the competitive cases.

$$U_n(z) = \sin K_n z \tag{1}$$

for which the cavity frequency

$$\Omega_n \equiv K_n c = n\pi c/L \ . \tag{2}$$

Here L is the length of the cavity, c is the speed of light, and n is a large integer on the order of 10^6. In general, the electric field has the expansion

$$E(z,t) = \frac{1}{2}\sum_n E_n(t)\exp[-i(\nu_n t + \phi_n)]U_n(z) + \text{c.c.} \ , \tag{3}$$

where the amplitude $E_n(t)$ and phase ϕ_n vary little in an optical frequency period. The corresponding induced polarization has the Fourier expansion

$$P(z,t) = \frac{1}{2}\sum_n \mathcal{P}_n(t)\exp[-i(\nu_n t + \phi_n)]U_n(z) + \text{c.c.} \ , \tag{4}$$

where the complex polarization $\mathcal{P}_n(t)$ is slowly varying in time. The electromagnetic field in the cavity satisfies Maxwell's equations. We demand that the field be self-consistent, that is, that the field assumed to induce polarization of the active medium be equal to the field produced by that polarization according to Maxwell's equations. In standard fashion[4] we combine Eqs. (3) and (4) with Maxwell's equations and get the self-consistency equations

$$\dot{E}_n = -\tfrac{1}{2}(\nu_n/Q_n)E_n - \tfrac{1}{2}(\nu_n/\epsilon_0)\,\mathrm{Im}(\mathcal{P}_n) \ , \tag{5}$$

$$\nu_n + \dot{\phi}_n = \Omega_n - \tfrac{1}{2}(\nu_n/\epsilon_0)E_n^{-1}\,\mathrm{Re}(\mathcal{P}_n) \ , \tag{6}$$

where ϵ_0 is the permittivity of free space and Q_n is the quality factor of the cavity for mode n.

We calculate the polarizations $\mathcal{P}_n$ from quantum mechanics using a (3×3) population matrix (an unnormalized density matrix whose diagonal elements yield level populations). The rate-equations approximation often used in laser theory here yields nine linear equations for the population matrix elements which are not readily solved exactly by analytical techniques. Two elements represent coherence between levels of a forbidden transition (e.g., levels 3 and 1 in the cascade case). This coherence results from two interactions of the electric field and is referred to as an electric-quadrupole term (the electric-quadrupole operator has a nonzero matrix element). It introduces additional terms in the equations of motion. Hence, the perturbation method is followed, and, in general, terms like ρ_{31} (population matrix component) in the cascade case are nonzero in second (and higher) order. Computer analysis of two-mode operation of both homogeneously broadened and gas lasers is done in each case. We find that the mode coupling is quite weak, i.e., the modes saturate themselves considerably more than one another and, hence, oscillate almost independently. Moreover, in the cascade case, the terms coupling the modes result in mutual aid rather than the usual competition leading to a reduction in errors originating from third-order theory and a small peak in the center of the Lamb dip in the Doppler-broadened case.

In Sec. II general equations of motion for the population matrix are derived and the relationships between matrix components and the polarizations $\mathcal{P}_n$ are given. In Sec. III the equations for the cascade and the competitive cases, respectively, for homogeneously broadened media are solved in detail. Appendix A gives a derivation of the case for an arbitrary amount of Doppler broadening and for simple running-wave cases. In Sec. IV the amplitude- and frequency-determining equations for both cases are given along with tables of coefficients. Section V discusses the validity of the third-order theory, revealing that errors incurred through neglect of higher-order terms tend to cancel one another for cascade transitions. Section VI presents steady-state numerical solutions. Section VII generalizes the three-level cascade treatment to $N+1$ levels possibly sustaining N modes of the radiation field. Specifically, a distinct mode is associated with each pair of levels. In Appendix B the relationship between this simple model and the anharmonic cascades encountered in diatomic molecules such as CO is discussed. The section closes with multimode numerical results.

II. POLARIZATION OF THE HOMOGENEOUSLY BROADENED AND DOPPLER-BROADENED MEDIA

We represent the atom-field interaction by the electric dipole perturbation energy

$$\mathcal{V} = -e\vec{r}\cdot\vec{E} \ . \tag{7}$$

In the rotating-wave approximation (RWA) for cascade case, this energy has matrix elements [see Fig. 1(a)]

$$\mathcal{V}_{32} = -\tfrac{1}{2}\wp_{32}E_2(t)\exp[-i(\nu_2 t + \phi_2)]U_2(z) \ , \tag{8}$$

$$\mathcal{V}_{21} = -\tfrac{1}{2}\wp_{21}E_1(t)\exp[-i(\nu_1 t + \phi_1)]U_1(z) \ , \tag{9}$$

where $\wp_{32}(\wp_{21})$ is the electric dipole matrix element between the 3 and 2 (2 and 1) levels. For the competitive case, $\mathcal{V}_{23} = \mathcal{V}_{32}$ with the change $\wp_{32} \to \wp_{23}$. The $\wp$'s are taken to be real, without loss of generality. In general, the equation of motion for the population matrix is given by

$$\dot{\rho} = \lambda - (i/\hbar)[\mathcal{H},\rho] - \tfrac{1}{2}[\Gamma\rho + \rho\Gamma] \ , \tag{10}$$

where $\mathcal{H}$ is the total Hamiltonian of the system, $\Gamma_{ij} = \gamma_i\delta_{ij}$ for which γ_i is the decay rate of the level i, and $\lambda_{ij} = \lambda_i\delta_{ij}$ where λ_i is the pump rate to the level i (assumed to vary little in an atomic lifetime). Along the lines for a two-level medium,[4]

we obtain the component equations of motion for the population matrix for each case. For either type of transition, $\mathcal{V}_{31}$ is zero so that

$$\dot{\rho}_{32} = -(i\omega_{32}+\gamma_{32})\rho_{32} + (i/\hbar)\mathcal{V}_{32}(\rho_{33}-\rho_{22}) + (i/\hbar)\mathcal{V}_{12}\rho_{31} , \tag{11}$$

$$\dot{\rho}_{21} = -(i\omega_{21}+\gamma_{21})\rho_{21} + (i/\hbar)\mathcal{V}_{21}(\rho_{22}-\rho_{11}) - (i/\hbar)\mathcal{V}_{23}\rho_{31} , \tag{12}$$

$$\dot{\rho}_{31} = -(i\omega_{31}+\gamma_{31})\rho_{31} - (i/\hbar)(\mathcal{V}_{32}\rho_{21} - \rho_{32}\mathcal{V}_{21}) , \tag{13}$$

$$\dot{\rho}_{33} = \lambda_3 - \gamma_3\rho_{33} - (i/\hbar)(\mathcal{V}_{32}\rho_{23} + \text{c.c.}) , \tag{14}$$

$$\dot{\rho}_{22} = \lambda_2 - \gamma_2\rho_{22} + [(i/\hbar)\mathcal{V}_{32}\rho_{23} + \text{c.c.}] - [(i/\hbar)\mathcal{V}_{21}\rho_{12} + \text{c.c.}] , \tag{15}$$

$$\dot{\rho}_{11} = \lambda_1 - \gamma_1\rho_{11} + [(i/\hbar)\mathcal{V}_{21}\rho_{12} + \text{c.c.}] , \tag{16}$$

where the frequencies ω_{32}, ω_{21}, and ω_{31} are shown in Fig. 1. To account approximately for collision effects, i.e., the dephasing time due to collisions, we include an addition $\gamma_{ij}^{\text{phase}}$, etc., in our definition of γ_{ij} in component equations defined by

$$\gamma_{ij} = \tfrac{1}{2}(\gamma_i+\gamma_j) + \gamma_{ij}^{\text{phase}} , \tag{17}$$

i.e., there is additional broadening due to collisions. The corresponding equations of motion for the competitive configuration [see Fig. 1(b)] are identical to (11)–(16). However, note that ω_{32} for the competitive case is negative leading to slight change in the resonant denominator resulting from the RWA. Note also that population inversions between states 2 and 3 have opposite signs in the two cases. The differences in the two cases are described explicitly in Table I of three-level coefficients. The off-diagonal element ρ_{31} represents the coherence generated by pairs of electric dipole interactions and contributes to the expectation value of the electric-quadrupole operator. In terms of the population matrix components, the complex polarization of (4) for the $n+1 \rightarrow n$ transition is given by

$$\mathcal{P}_n(t) = 2\exp[i(\nu_n t+\phi_n)] \times \frac{1}{M_n}\int_0^L dz U_n^*(z)\wp_{n+1,n}\rho_{n+1,n}(z,t) , \tag{18}$$

where M is the normalization constant

$$M_n = \int_0^L |U_n(z)|^2 dz . \tag{19}$$

We see that the off-diagonal elements like $\rho_{n+1,n}$ lead to polarization of the medium.

In a gas medium atoms move through the standing-wave electric field, seeing Doppler-shifted frequencies, or equivalently amplitude-modulated fields. (See Ref. 4, Chap. 10 for a detailed discussion.) Hence, in forming the macroscopic polarization $\mathcal{P}_n(t)$, one must include in (18) an integral over the velocity distribution. Specifically, the complex polarization $\mathcal{P}_n$ of Eq. (4) is given by

$$\mathcal{P}_n(t) = 2\wp_{n+1,n}\exp[(i\nu_n t+\phi_n)] \times \int_{-\infty}^{\infty} dv \frac{1}{M_n}\int_0^L dz U_n^*(z)\rho_{n+1,n}(z,v,t) . \tag{20}$$

Here, $\rho_{n+1,n}(z,v,t)$ obeys the same equations of motion as $\rho_{n+1,n}(z,t)$ with time derivative read as $\partial/\partial t + v(\partial/\partial z)$. The Doppler-broadened case is worked out in Appendix A.

III. INTEGRATION OF THE EQUATIONS OF MOTION

Following the perturbation method, we solve equations of motion up to third order in the electric field interaction and find the complex polarization (18). This is used in Eqs. (5) and (6) to obtain amplitude- and frequency-determining equations.

The population matrix off-diagonal elements are given by the formal integrals of (11)–(13), for example,

$$\rho_{32} = \frac{i}{\hbar}\int_{-\infty}^{t} dt' \exp[-(i\omega_{32}+\gamma_{32})(t-t')] \times [\mathcal{V}_{32}(z,t')(\rho_{33}-\rho_{22}) + \mathcal{V}_{12}\rho_{31}] . \tag{21}$$

In zeroth order (no perturbation), off-diagonal elements are zero while the diagonal elements (populations of levels) are given by

$$\rho_{\alpha\alpha}^{(0)} = \lambda_\alpha/\gamma_\alpha , \quad \alpha = 1, 2, 3, \tag{22}$$

and (unsaturated) population differences are given by

$$N_{\alpha,\alpha-1} = \rho_{\alpha\alpha}^{(0)} - \rho_{\alpha-1,\alpha-1}^{(0)} = \lambda_\alpha/\gamma_\alpha - \lambda_{\alpha-1}/\gamma_{\alpha-1} . \tag{23}$$

We iterate the calculation to third order with the assumption that the amplitudes E_n and phases ϕ_n of the electric field (3) vary sufficiently little in atomic lifetimes to be factored outside the time integrations. Using the zeroth-order difference (23) in the integral (21), we find the first-order contribution for ρ_{32} to be

$$\rho_{32}^{(1)} = -\tfrac{1}{2}(\wp_{32}/\hbar)N_{32}(z,t)E_2U_2\exp[-i(\nu_2 t+\phi_2)] \times [(\omega_{32}-\nu_2)+i\gamma_{32})]/[\omega_{32}-\nu_2)^2+\gamma_{32}^2] . \tag{24}$$

For the sake of brevity we write down the explicit formulas for the upper transition of the cascade case only. The corresponding formulas for

TABLE I. Summary of coefficients appearing in the amplitude- and frequency-determining Eqs. (37)–(40). $n=2$ refers to 32 transition and $n=1$ to other transition. The corresponding coefficients for $n=1$ mode are given by the values above with $2 \leftrightarrow 1$ and $32 \leftrightarrow 21$, $\gamma_3 \leftrightarrow \gamma_1$ for cascade, and $32 \leftrightarrow 12$, $\gamma_3 \leftrightarrow \gamma_1$ for competitive. The α, β, $F^{(1)}$, $F^{(3)}$, σ, ρ, and ϑ_{2222} coefficients are same for both cases and ϑ_{2211} and ϑ_{2112} are given separately. Terms here are defined as follows: the frequency ν_n (3); Q_n the cavity factor (Q) for mode n; ω_{32} (Fig. 1); $\wp_{32}$ is the electric dipole element of transition (8); $\mathfrak{L}_{32}$ is the Lorentzian (26); ϵ_0 is the permittivity of free space; γ_3, γ_2, and γ_1 are the decay constants of the levels 3, 2, and 1 and γ_{32} is the decay constant of the polarization induced between levels 3 and 2 (18); $\bar{N}_{32}$ is a population inversion of (35). Note the complex $\vartheta_{n\mu\rho\sigma}$ are used in general mode amplitude and frequency equations [see Eqs. (9–18) and (9–19), Chap. 9, Ref. 4].

Coefficient	Physical interpretation
$\alpha_2 = -\frac{1}{2}\nu_2/Q_2 + F_{32}^{(1)}\mathfrak{L}_{32}(\omega_{32}-\nu_2)$	linear net gain
$\beta_2 = \mathfrak{L}_{32}^2(\omega_{32}-\nu_2)F_{32}^{(3)}$	self-saturation
$F_{32}^{(1)} = \frac{1}{2}\nu_2\left(\frac{\wp_{32}^2}{\hbar\epsilon_0\gamma_{32}}\right)\bar{N}_{32}$	first-order factor
$F_{32}^{(3)} = \frac{3}{2}\left(\frac{\wp_{32}}{2\hbar}\right)^2\frac{1}{\gamma_{32}}F_{32}^{(1)}\left(\frac{1}{\gamma_3}+\frac{1}{\gamma_2}\right)$	third-order factor
$\sigma_2 = \frac{\omega_{32}-\nu_2}{\gamma_{32}}\mathfrak{L}_{32}(\omega_{32}-\nu_2)F_{32}^{(1)}$	linear mode pulling
$\rho_2 = \left(\frac{\omega_{32}-\nu_2}{\gamma_{32}}\right)\mathfrak{L}_{32}^2(\omega_{32}-\nu_2)F_{32}^{(3)}$	self-pushing
$\vartheta_{2211} = -\frac{1}{8}i\nu_2[(\wp_{32}\wp_{21})^2\bar{N}_{21}/(\hbar^3\epsilon_0\gamma_2\gamma_{21})] \times\mathfrak{D}_{32}(\omega_{32}-\nu_2)\mathfrak{L}_{21}(\omega_{21}-\nu_1)$	complex cross-saturation population depletion part (cascade)
$\vartheta_{2112} = -\frac{1}{8}F_{32}^{(1)}\gamma_{32}(\wp_{21}/\hbar)^2\mathfrak{D}_{32}(\omega_{32}-\nu_2)\mathfrak{D}_{31}(\omega_{31}-\nu_1-\nu_2) \times[(\bar{N}_{21}/\bar{N}_{32})\mathfrak{D}_{21}(\omega_{21}-\nu_1)-\mathfrak{D}_{32}(\omega_{32}-\nu_2)]$	complex cross-saturation quadrupole part (cascade)
$\vartheta_{2211} = \frac{1}{8}i\nu_2[(\wp_{32}\wp_{31})^2\bar{N}_{21}/(\hbar^3\epsilon_0\gamma_3\gamma_{31})] \times\mathfrak{D}_{32}(\omega_{32}-\nu_2)\mathfrak{L}_{31}(\omega_{31}-\nu_1)$	complex cross-saturation population depletion part (competitive)
$\vartheta_{2112} = \frac{1}{8}iF_{32}^{(1)}\gamma_{32}(\wp_{31}/\hbar)^2\mathfrak{D}_{32}(\omega_{32}-\nu_2)\,\mathfrak{D}_{21}(\nu_1-\nu_2-\omega_{21}) \times[(\bar{N}_{31}/\bar{N}_{32})\mathfrak{D}_{31}(\nu_1-\omega_{31})+\mathfrak{D}_{32}(\omega_{32}-\nu_2)]$	complex cross-saturation electric-quadrupole part (competitive)
$\tau_{nm}+i\theta_{nm}=\vartheta_{nnmm}+\vartheta_{nmmn}$	cross-saturation terms

the other transition and the competitive cases can easily be derived from them and are identical for both cascade and competitive $2\rightarrow 1$ transition. Also we find $\rho_{31}^{(1)}=0$. The diagonal elements have vanishing contributions in first order, because excitation to a superposition of levels is assumed not to occur. Substituting the first-order contributions into the equations of motion (11)–(16), we get, for example, (accurate to second order)

$$\dot{\rho}_{33} \approx \lambda_3 - \gamma_3\rho_{33} - [\tfrac{1}{2}(\wp_{32}/\hbar)^2(N_{32}/\gamma_{32})E_2^2|U_2|^2 \times\mathfrak{L}_{32}(\omega_{32}-\nu_2)] , \quad (25)$$

where $\mathfrak{L}_{32}(\omega_{32}-\nu_2)$ is a special case of the Lorentzian function defined by

$$\mathfrak{L}_x(\Delta\omega) = \gamma_x^2/[\gamma_x^2+(\Delta\omega)^2] . \quad (26)$$

We denote the term in the square brackets of (25) by $N_{32}R_{32}$ (R_{32} has the form of a rate constant), that is,

$$R_{32} \equiv \tfrac{1}{2}(\wp_{32}/\hbar)^2(1/\gamma_{32})E_2^2|U_2|^2\mathfrak{L}_{32}(\omega_{32}-\nu_2) . \quad (27)$$

R_{21} is given by R_{32} with $3\rightarrow 2$ and $2\rightarrow 1$. In terms of the R's, the second-order contributions for the populations are

$$\rho_{33}^{(2)} = -N_{32}R_{32}/\gamma_3 , \quad (28)$$

$$\rho_{22}^{(2)} = N_{32}R_{32}/\gamma_2 - N_{21}R_{21}/\gamma_2 , \quad (29)$$

$$\rho_{11}^{(2)} = N_{21}R_{21}/\gamma_1 . \quad (30)$$

The electric dipole elements ρ_{32} and ρ_{21} have vanishing contributions in second order, but the "electric-quadrupole" term ρ_{31} has the contribution

$$\rho_{31}^{(2)} = \tfrac{1}{4}(\wp_{32}\wp_{21}/\hbar^2)E_1U_1E_2U_2\exp[-i(\nu_1t+\nu_2t+\phi_1+\phi_2)] \times[N_{21}\mathfrak{D}_{21}(\omega_{21}-\nu_1)-N_{32}\mathfrak{D}_{32}(\omega_{32}-\nu_2)] \times\mathfrak{D}_{31}(\omega_{31}-\nu_1-\nu_2)\ . \tag{31}$$

Here the complex denominator

$$\mathfrak{D}_x(\Delta\omega)=[\gamma_x+i(\Delta\omega)]^{-1}\ . \tag{32}$$

The third-order contributions to the populations and electric quadrupole are zero. We find the third-order polarization element $\rho_{32}^{(3)}$ to be

$$\rho_{32}^{(3)} = \tfrac{1}{2}i\exp[-i(\nu_2t+\phi_2)]\mathfrak{D}_{32}(\omega_{32}-\nu_2)(\wp_{32}/\hbar)E_2U_2\{(1/\gamma_3+1/\gamma_2)N_{32}R_{32}-N_{21}R_{21}/\gamma_2-\tfrac{1}{4}(\wp_{21}/\hbar)^2E_1^2|U_1|^2 \times\mathfrak{D}_{31}(\omega_{31}-\nu_1-\nu_2)[N_{21}\mathfrak{D}_{21}(\omega_{21}-\nu_1)-N_{32}\mathfrak{D}_{32}(\omega_{32}-\nu_2)]\}\ , \tag{33}$$

and $\rho_{21}^{(3)}$ is given by $\rho_{32}^{(3)}$ with the following interchanges: (i) subscripts $1\rightarrow 2$ on the field variables in Eq. (3), (ii) the subscript pair $32\rightarrow 21$ wherever it appears, and (iii) $\gamma_1\rightarrow\gamma_3$. Using (18) we get the first-order polarization

$$\mathcal{P}_2^{(1)}(t) = -(\wp_{32}^2/\hbar)\bar{N}_{32}E_2\frac{(\omega_{32}-\nu_2)+i\gamma_{32}}{(\omega_{32}-\nu_2)^2+\gamma_{32}^2}\ , \tag{34}$$

where $\bar{N}_{32}$ is given by the $n=2$ case of the expression

$$\bar{N}_{n+1,n}=\frac{1}{M_n}\int_0^L|U_n(z)|^2N_{n+1,n}(z,t)dz \cong\frac{1}{L}\int_0^L N_{n+1,n}(z,t)dz\ . \tag{35}$$

Here, we have discarded terms in (35) which vary rapidly in z, i.e., $\cos 2K_nz$. No approximation is involved here for the running-wave case. The expression for $\mathcal{P}_1^{(1)}(t)$ is derived from Eqs. (34) and (35) by the interchanges $2\rightarrow 1$ and $3\rightarrow 2$. The third-order contributions contain similar spatial integrals which are treated in substantially the same way. Unlike normal two-mode theories, the terms varying as $\cos(K_1-K_2)z$ are also rapidly varying, since they refer to different transitions rather than neighboring modes in a cavity.

We find the third-order contribution of the polarization of the second mode to be [combining (18) with (33)]

$$\mathcal{P}_2^{(3)}(t) = \tfrac{1}{4}i\mathfrak{D}_{32}(\omega_{32}-\nu_2)(\wp_{32}^2/\hbar)E_2\{\tfrac{3}{2}(\wp_{32}/\hbar)(\bar{N}_{32}/\gamma_{32})E_2^2(1/\gamma_3+1/\gamma_2)\mathfrak{L}_{32}(\omega_{32}-\nu_2) -(1/\gamma_2)(\wp_{21}/\hbar)^2E_1^2(\bar{N}_{21}/\gamma_{21})\mathfrak{L}_{21}(\omega_{21}-\nu_1) -\tfrac{1}{2}(\wp_{21}/\hbar)^2E_1^2\mathfrak{D}_{31}(\omega_{31}-\nu_1-\nu_2)[\bar{N}_{21}\mathfrak{D}_{21}(\omega_{21}-\nu_1)-\bar{N}_{32}\mathfrak{D}_{32}(\omega_{32}-\nu_2)]\}\ . \tag{36}$$

$\mathcal{P}_1^{(3)}(t)$ is given by $\mathcal{P}_2^{(3)}(t)$ with the interchanges applied to (33) for $\rho_{21}^{(3)}$. $\mathcal{P}_2^{(3)}(t)$ for the competitive case can be obtained by taking the complex conjugate of (36) provided we let $\nu_2\rightarrow-\nu_2$ and note that $\omega_{32}=-\omega_{23}$ and $N_{23}=-N_{32}$. The total polarization accurate to third order is given by the sum of $\mathcal{P}^{(1)}(t)$ and $\mathcal{P}^{(3)}(t)$. Thus, combining the polarization contributions (34) and (36) with the self-consistency Eqs. (5) and (6), we can find equations that determine the field amplitudes and frequencies (i.e., in Sec. IV). More general results allowing for Doppler broadening are given in Appendix A. The derivation there requires understanding of the perturbation tree technique (see, for example, Chap. 10 and Appendix D of Ref. 4) not used here for the simpler homogeneously broadened medium.

IV. AMPLITUDE- AND FREQUENCY-DETERMINING EQUATIONS: FORMAL STEADY-STATE SOLUTIONS

Using the complex polarization up to third order for each case and the self-consistency equations (5) and (6), we find the amplitude-determining equations

$$\dot{E}_1=E_1(\alpha_1-\beta_1E_1^2-\theta_{12}E_2^2)\ , \tag{37}$$

$$\dot{E}_2=E_2(\alpha_2-\beta_2E_2^2-\theta_{21}E_1^2)\ , \tag{38}$$

and the frequency-determining equations

$$\nu_1+\dot{\phi}_1=\Omega_1+\sigma_1-\rho_1E_1^2-\tau_{12}E_2^2\ , \tag{39}$$

$$\nu_2+\dot{\phi}_2=\Omega_2+\sigma_2-\rho_2E_2^2-\tau_{21}E_1^2\ . \tag{40}$$

The coefficients for the homogeneous cases are given in Table I and for the inhomogeneous cases in Table II. In the cascade case the θ's and τ's have opposite signs to the usual two-mode transitions. In essence the two transitions help each other to lase rather than compete. This can be seen from a physical point of view in that mode 2 (the upper transition) populates the middle laser level which is the upper level for mode 1, that is, mode 2 increases the population inversion for mode 1. Similarly, mode 1 depopulates the lower level for mode 2, increasing the latter's inversion.

The analysis of steady-state operation is considerably simplified through the use of the intensities $I_n = E_n^2$. Multiplying (37) and (38) by $2E_1$ and $2E_2$, respectively, we find the equations of motion

$$\dot{I}_1 = 2I_1(\alpha_1 - \beta_1 I_1 - \theta_{12} I_2) \tag{41}$$

$$\dot{I}_2 = 2I_2(\alpha_2 - \beta_2 I_2 - \theta_{21} I_1) \,. \tag{42}$$

Stationary solutions occur when $\dot{I}_1 = \dot{I}_2 = 0$. Physical solutions of interest are those for which intensities are non-negative and stable. Conditions for stability for the competitive case are identical to those for normal two-mode theory discussed in Ref. 4, Chap. 9-2. The coupling constant

$$C = \theta_{12}\theta_{21}/\beta_1\beta_2 \tag{43}$$

expresses the degree to which the modes are coupled. $C < 1$ defines weak coupling, $C = 1$ neutral coupling, and $C > 1$ strong coupling. In Appendix A of Ref. 10, more general conditions for stable solutions are discussed. It is shown that for the cascade case when $C \geq 1$, no stable solution exists. This point is interpreted in Sec. V. It is convenient to express the coefficients in terms of the relative excitation defined by

$$\mathfrak{N} = \bar{N}/\bar{N}_T \,, \tag{43a}$$

where $\bar{N}_T$ is the value of the population inversion $\bar{N}$ at threshold (given by $\alpha = 0$ for central tuning). In describing our numerical examples (Sec. VI), we use $\mathfrak{N}_1$ and $\mathfrak{N}_2$, for which the $\bar{N}_T$ are defined by α_1, $\alpha_2 = 0$, respectively. We turn now to a stability discussion for the cascade case.

TABLE II. Coefficients appearing in the amplitude- and frequency-determining equations (37)–(40), for the Doppler limit for the 32 transition. For further explanation refer to the caption of Table I.

Coefficient	Physical interpretation
$\alpha_2 = -\frac{1}{2}\frac{\nu_2}{Q_2} + F_{32}^{(1)} \exp[-(\omega_{32} - \nu_2)^2/(Ku)^2]$	linear net gain
$\beta_2 = [1 + \mathfrak{L}_{32}(\omega_{32} - \nu_2)]\, F_{32}^{(3)}$	self-saturation for $n = 2$
$F_{32}^{(1)} = \frac{1}{2}\pi^{1/2}\nu_2[\wp_{32}^2/(\hbar\epsilon_0 Ku)]\, \bar{N}_{32}$	first-order factor
$F_{32}^{(3)} = \frac{1}{4}(\frac{1}{2}\wp_{32}/\hbar)^2(\gamma_3^{-1} + \gamma_2^{-1})\gamma_{32}^{-1} F_{32}^{(1)}$	third-order factor
$\sigma_2 = \frac{1}{2}(\nu_2/\epsilon_0)\wp_{32}^2 (Ku\hbar)^{-1}\bar{N}_{32}\,\mathrm{Re}\,\mathfrak{z}[\gamma_{32} + i(\omega_{32} - \nu_2)]$	linear mode pulling
$\mathfrak{z}(v) = \frac{-iK}{\pi^{1/2}}\int_{-\infty}^{\infty} dv\, e^{-(v/u)^2}/(v + iKv)$	plasma dispersion function
$\rho_2 = [(\omega_{32} - \nu_2)/\gamma_{32}]\, \mathfrak{L}_{32}(\omega_{32} - \nu_2) F_{32}^{(3)}$	self-pushing
$\vartheta_{2211} = \frac{1}{16} i\pi^{1/2}\nu_2[(\wp_{32}\wp_{21})^2\bar{N}_{21}/\hbar^3\epsilon_0\gamma_2 Ku]$ $\times[\mathfrak{D}_{32+21}(\omega_{31} - \nu_1 - \nu_2) + \mathfrak{D}_{32+21}(\omega_{32} - \omega_{21} - \nu_2 + \nu_1)]$	complex cross-saturation population depletion part (cascade)
$\vartheta_{2112} = \frac{1}{16} i\pi^{1/2}\nu_2[(\wp_{32}\wp_{21})^2\bar{N}_{21}/\hbar^3\epsilon_0 Ku]$ $\times\mathfrak{D}_{31}(\omega_{31} - \nu_1 - \nu_2)\,\mathfrak{D}_{32+21}(\omega_{31} - \nu_1 - \nu_2)$	complex cross-saturation quadrupole part (cascade)
$\vartheta_{2211} = \frac{1}{16} i\nu_2\pi^{1/2}[(\wp_{32}\wp_{31})^2\bar{N}_{21}/\hbar^3\epsilon_0\gamma_3 Ku]$ $\times[\mathfrak{D}_{32+31}(\omega_{32} + \omega_{31} - \nu_1 - \nu_2) + \mathfrak{D}_{32+31}(\omega_{32} - \omega_{31} - \nu_2 + \nu_1)]$	complex cross-saturation population depletion part (competitive)
$\vartheta_{2112} = \frac{1}{16} i\nu_2\pi^{1/2}[(\wp_{32}\wp_{31})^2\bar{N}_{21}/\hbar^3\epsilon_0 Ku]$ $\times\mathfrak{D}_{21}(\omega_{32} - \omega_{31} + \nu_1 - \nu_2)\,\mathfrak{D}_{32+31}(\omega_{32} - \omega_{31} + \nu_1 - \nu_2)$	complex cross-saturation quadrupole part (competitive)

V. DISCUSSION OF THIRD-ORDER CASCADE THEORY

In Sec. IV we noted that certain special problems may arise in the formal solution of the equations of motion in the cascade case. In particular, two-mode third-order theories are characterized by the coupling constant C [Eq. (43)], which determines the stable solutions of the equations, depending on whether C is greater than or less than unity (strong versus weak coupling). The coupling constant, which is always positive, comes into the solutions as a term $(1-C)$ in the denominator (see Ref. 4, Chap. 9-2). This is apparently singular for $C=1$, but in all cases except the cascade, the numerator also vanishes thereby removing the singularity. In the cascade case, the third-order theory is actually singular for $C=1$. In addition, for strong coupling ($C>1$), the third-order theory gives results that are nonphysical, namely unsaturable exponential buildup, even when both modes are below threshold. This is due to the larger size and opposite sign (providing gain) of the cross-saturation terms (θ's) relative to the self-saturation (β's) in Eqs. (41) and (42).

In this section we use a simplified model of a homogeneously broadened unidirectional ring laser to explore the validity of the third-order theory in the regime of $C \lesssim 1$. We use this model since spatial dependences cancel out and, with only a few approximations, the corresponding exact theory can be solved in closed form. We find two key results: First, that strong coupling does not appear to be likely in the cascade case (although it may occur for multilevel bidirectional operation as discussed in Appendix A); secondly, for C near 1, one can use the third-order theory even if the laser is not particularly close to threshold and expect to get reasonable results. This second result is due to the fact that neglected higher-order self-saturation terms tend to be canceled by corresponding higher-order cross-saturation terms, particularly as the two phenomena approach one another in magnitude ($C \to 1$).

In order to obtain an exact solution for the homogeneously broadened unidirectional ring laser, it is necessary to ignore the quadrupole terms, i.e., ρ_{31}. We note that these terms tend to cancel out in the homogeneously broadened case (see ϑ_{2112} in Table I), so ignoring them should not be serious. Without them, Eqs. (11)–(16) give on resonance and in the rate-equation approximation (see Chap. 8-2 of Ref. 4),

$$\dot{\rho}_{11} = \lambda_1 - \gamma_1\rho_{11} + (\wp_{12}^2 I_1/2\hbar^2\gamma_{12})(\rho_{22}-\rho_{11}), \tag{44}$$

$$\dot{\rho}_{22} = \lambda_2 - \gamma_2\rho_{22} - (\wp_{12}^2 I_1/2\hbar^2\gamma_{12})(\rho_{22}-\rho_{11}) + (\wp_{23}^2 I_2/2\hbar^2\gamma_{23})(\rho_{33}-\rho_{22}), \tag{45}$$

$$\dot{\rho}_{33} = \lambda_3 - \gamma_3\rho_{33} - (\wp_{23}^2 I_2/2\hbar^2\gamma_{23})(\rho_{33}-\rho_{22}). \tag{46}$$

We also write the equations for the time evolution of the intensities as

$$dI_1/dt = g_1(\rho_{22}-\rho_{11})I_1 - (\nu_1/Q_1)I_1, \tag{47}$$

$$dI_2/dt = \pm g_2(\rho_{33}-\rho_{22})I_2 - (\nu_2/Q_2)I_2, \tag{48}$$

where g_n is the small signal gain of the nth mode defined by $\alpha_n = g_n\bar{N}_{n+1,n} - \nu_n/Q_n$ for central tuning. The plus sign in Eq. (48) is for the cascade and the negative sign for the competitive case. The equations for the population can be solved in steady state with straightforward algebra. For typographical simplicity, we introduce the dimensionless intensity

$$\mathcal{I}_n = \left(\frac{1}{\gamma_{n+1}} + \frac{1}{\gamma_n}\right)\frac{\wp_{n+1,n}^2}{2\hbar^2\gamma_{n+1,n}} I_n,$$

and use the relative excitations defined by Eq. (44). We find the equation of motion

$$\frac{d\mathcal{I}_1}{dt} = \mathcal{I}_1 \frac{(\nu_1/Q_1)\mathfrak{N}_1(1+\mathcal{I}_2) + (\nu_2/Q_2)\mathfrak{N}_2(g_1/g_2)\mathcal{I}_2\gamma_3/(\gamma_3+\gamma_2)}{(1+\mathcal{I}_1)(1+\mathcal{I}_2) - \mathcal{I}_1\mathcal{I}_2[\gamma_1\gamma_3/(\gamma_1+\gamma_2)(\gamma_2+\gamma_3)]} - \frac{\nu_1}{Q_1}\mathcal{I}_1. \tag{49}$$

The equation for the second mode is found by interchanging $\gamma_3 \rightleftarrows \gamma_1$ and $1 \rightleftarrows 2$ in the $\mathcal{I}_n$, ν_n/Q_n, and $\mathfrak{N}_n$.

The corresponding third-order expression is found by expanding the exact results to third order to give

$$\dot{\mathcal{I}}_n = 2\mathcal{I}_n[\alpha_n - \beta_n\mathcal{I}_n - \theta_{nm}\mathcal{I}_m], \tag{50}$$

where $n=1,2$, $m=2,1$, and the self-saturation coefficients are

$$\beta_n = (\nu_n/Q_n)\mathfrak{N}_n \tag{51}$$

and the cross-saturation coefficients are

$$\theta_{12} = \frac{\nu_2}{Q_2}\mathfrak{N}_2\frac{g_1}{g_2}\frac{\gamma_3}{\gamma_3+\gamma_2} \tag{52}$$

and

$$\theta_{21} = \frac{\nu_1}{Q_1}\mathfrak{N}_1\frac{g_2}{g_1}\frac{\gamma_1}{\gamma_1+\gamma_2}. \tag{53}$$

The coupling constant is, therefore,

$$C = \frac{\theta_{12}\theta_{21}}{\beta_1\beta_2} = \frac{\gamma_1\gamma_3}{(\gamma_1+\gamma_2)(\gamma_2+\gamma_3)}, \tag{54}$$

which is always less than one. It seems to be generally the case that C is less than one. For example, the standing-wave laser in this case gives

$$C = \frac{4}{9}\frac{\gamma_1\gamma_3}{(\gamma_1+\gamma_2)(\gamma_2+\gamma_3)}. \tag{55}$$

In our numerical computations we find reasonable values of C which tend to be smaller than 0.3. Thus, although it cannot be proved, we have been unable to find a common case in which the singularity actually occurs. The bidirectional case for which C might equal or exceed unity (see Appendix A) is probably not obtainable in any straightforward fashion experimentally.

The question still remains of what happens to the third-order results in the neighborhood of the singular point $C=1$. Although one would imagine that the theory would have little validity there, we find that just the opposite is the case. In fact, for values of $C \lesssim 1$, the third-order results remain reasonably accurate for far larger values of the relative excitation than one can reasonably use in ordinary single or multimode third-order calculations. A particular example is given in Figs. 2 and 3 which comes from solving Eqs. (42) and (49) in steady state for the case where $\gamma_1=\gamma_2=\gamma_3$ ($C=\frac{1}{4}$). One sees there that for one mode at threshold and the other substantially above, the third-order and exact answers are the same. The other mode is off by about 28% at a relative excitation of 1.5, with an overall accuracy of 14%. By comparison, a single-mode calculation for the same relative excitation would be off by 33%. We have tested many other cases with values of C in this range and have found these accuracies to be representative.

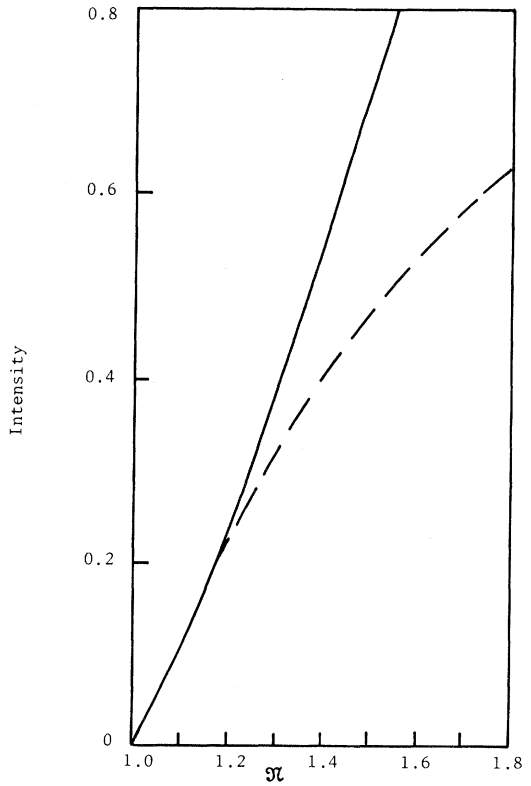

FIG. 2. Graphs of intensities of the exact (solid line) and the third-order (dashed line) cascade case for mode 1 versus $\mathfrak{N}$. $\mathfrak{N}$ is fixed at 1.0 (threshold value) and $\gamma_2/\gamma_3=\gamma_2/\gamma_1=1.0$.

VI. THREE-LEVEL NUMERICAL RESULTS

In this section we report computer analysis of the intensity equations (41) and (42) for both homogeneous and gas cases, yielding plots of mode intensities versus cavity detuning. The intensity of mode n is given in units of $\frac{1}{2}(\wp/\hbar)^2(\gamma_n\gamma_{n+1})^{-1}$ for convenience. We discuss the homogeneous case first. For the competitive transitions the coupling constant C of (43) has a maximum of about 0.3 at resonance falling off by 10% at 100 MHz off resonance, and for the cascade transitions it is practically a constant about 0.068 (very weak). For relative excitations $\mathfrak{N}_1=\mathfrak{N}_2=1.2$, the two modes oscillate almost independently of each other (Figs. 4 and 5). We see that in the cascade case (Fig. 4), the intensity of mode 1 oscillating alone is about 21% less than the two modes oscillating together, while in the competitive case (Fig. 5), it is about 35% more than the two-mode transitions. This illustrates the fact that cascade transitions help one another. If one of the modes is exactly at threshold, the presence of the other allows it to lase. We find, however, that a relative excitation of

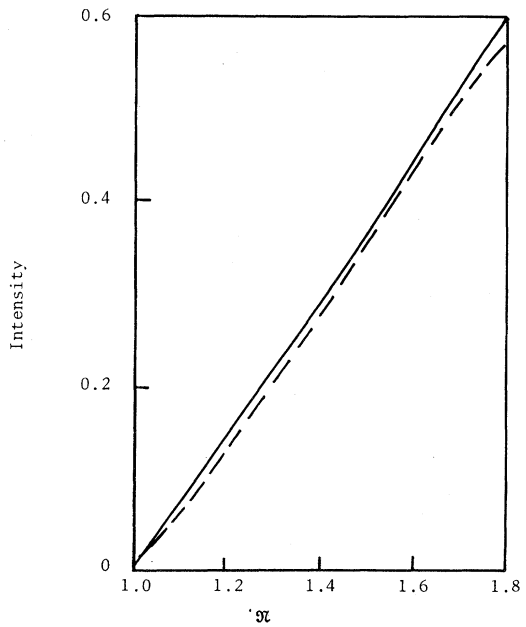

FIG. 3. Graphs of intensities of the exact (dashed line) and the third-order (solid line) cascade case for mode 2 versus $\mathfrak{N}$. $\mathfrak{N}$ is fixed at 1.0 (threshold value) and $\gamma_2/\gamma_3=\gamma_2/\gamma_1=1.0$. The two graphs are almost superimposed.

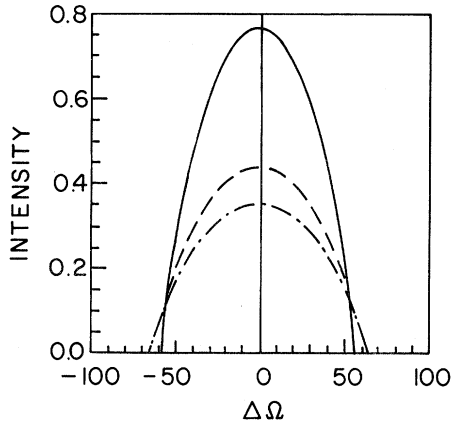

FIG. 4. Graph of three-level cascade transitions versus cavity detuning (which is about the same for both modes), homogeneously broadened stationary atoms. Solid line and dashed lines correspond to 32 and 21 transitions of Fig. 1(a), and the dashed-dotted line is the single-mode intensity of 21 transition. Laser parameters used are $\gamma_3 = 15.5$, $\gamma_2 = 41.0$, $\gamma_1 = 51.0$, $\gamma_{32} = 128.0$, $\gamma_{21} = 146.0$, $\gamma_{31} = 133.0$ MHz, and $\mathfrak{N}_1 = \mathfrak{N}_2 = 1.2$ [Eq. (43a)]. The 32 transition here rises substantially above the 21 transition due to the difference in scaling involved in the dimensionless intensities.

0.98 (less than threshold) for one mode and 1.2 for the other is not enough to bring the first mode above threshold. With excitation levels of 1.2 and 1.05, in the cascade case the second mode starts to oscillate close to resonance (Fig. 6) (and of course with much less intensity), while in the competitive case the first mode suppresses the second for all frequencies.

Figures 7 and 8 show the inhomogeneously broadened case results corresponding to Figs. 4 and 5. In the competitive transitions (Fig. 8), we see a simple Lamb dip at resonance with the intensity of mode 1 53% smaller than when oscillating alone. In the cascade case (Fig. 7), when the two modes are oscillating together, the mutual aid at resonance yields small peaks at the center of the Lamb dips. The intensity of the mode 1 oscillating alone is about 40% less than its intensity oscillating together with the other mode. In fact, the coupling constant for the cascade case is about 0.15 with a 25% increase at line center, explaining the appearance of the small peaks. This effect is more clearly observed with the excitation parameters of 1.2 and 1.05 (Fig. 9), where mode 2 shows no dip

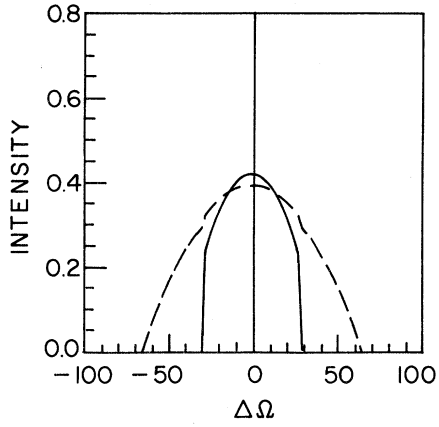

FIG. 6. Graph of cascade transitions versus cavity detuning, homogeneous case, for $\mathfrak{N}_2 = 1.05$. All the rest of the parameters are the same as in Fig. 4. This mode starts to oscillate only close to resonance.

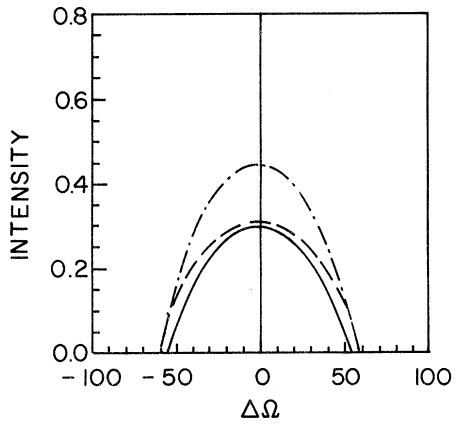

FIG. 5. Graph of three-level competitive transitions versus cavity detuning (same for both modes) for homogeneously broadened stationary atoms. Solid line and dashed line correspond to 23 and 21 transitions of Fig. 1(b), and the dashed-dotted line is the single-mode intensity of 21 transition. Laser parameters used are $\gamma_1 = 51.0$, $\gamma_{32} = 128.0$, $\gamma_{31} = 146.0$, and $\gamma_{21} = 133.0$ MHz and $\mathfrak{N}_1 = \mathfrak{N}_2 = 1.2$ [Eq. (43a)].

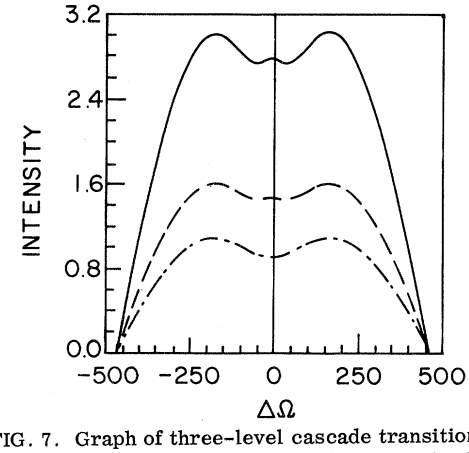

FIG. 7. Graph of three-level cascade transitions versus cavity detuning (which is about the same for both modes), inhomogeneously broadened medium. Solid line and dashed lines correspond to 32 and 21 transitions of Fig. 1(a) and the dashed-dotted line is the single-mode intensity of 21 transition. Laser parameters used are the same as in Fig. 4, plus a Doppler broadening of $Ku = 1010$ MHz.

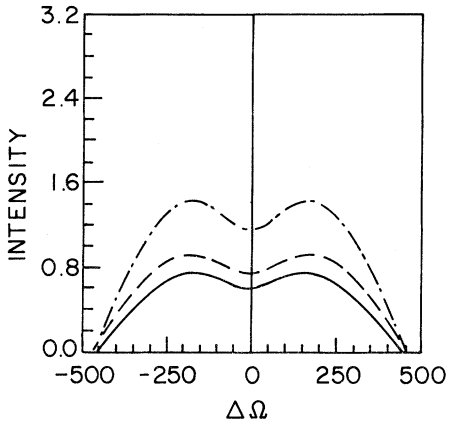

FIG. 8. Graph of three-level competitive transitions versus cavity detuning (same for both modes) for inhomogeneously broadened medium. Solid line and dashed line correspond to 23 and 21 transitions of Fig. 1(b), and the dashed-dotted line is the single-mode intensity of the 21 transition. The substantially larger value of this single-mode intensity is explained by the larger coupling of $C \simeq 0.65$. Laser parameters used are the same as in Fig. 5, plus a Doppler broadening of $Ku = 1010$ MHz.

at all. In contrast to the homogeneous case a relative excitation of 1.2 for mode 2 is enough to start the first mode pumped just to $\mathfrak{R}_1 = 0.98$ to lase. Figures 10 and 11 are two-mode plots at excitation levels of 1.2 and detuned by 50 MHz from each other. The cascade transitions start oscillating about 50 MHz apart, while the effect of competition prohibits the other competitive mode from oscillating until about 250 MHz apart.

Finally, we found that neglect of the coherence terms (particularly in cascade case with same relative excitations for both modes) leads to essentially the same results for the homogeneous transitions, but leads to loss of the small peak observed in the center of the Lamb dip in Figs. 9 and 10.

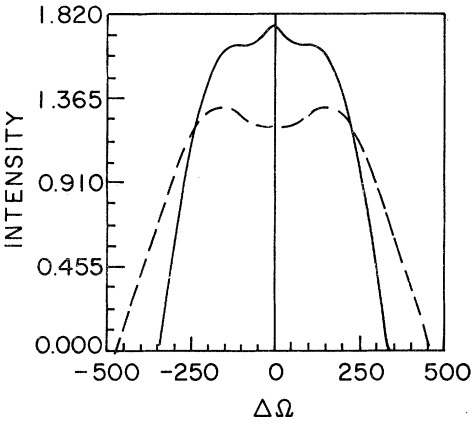

FIG. 9. Graph of cascade transitions versus cavity detuning, inhomogeneous case, for $\mathfrak{R}_2 = 1.05$ (solid line). All the rest of the parameters are the same as in Fig. 7.

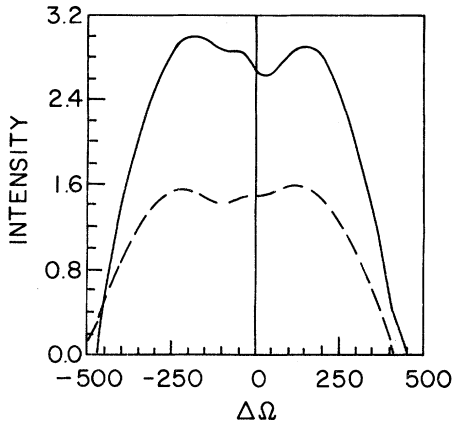

FIG. 10. Graph of three-level cascade transitions versus cavity detuning for the gas case with the two transitions detuned from each other by 50 MHz. Solid line and dashed lines correspond to 32 and 21 transitions of Fig. 1(a). Laser parameters are same as in Fig. 7.

Hence, this interesting effect in the cascade case is solely due to the coherence term ρ_{31}.

VII. MULTILEVEL CASCADE MODEL

In the present section we consider an $N+1$ level cascade (Fig. 12). In doing so, we wish to make connection with multiple-level cascades in diatomic molecules. We thus generalize the three-level system to an anharmonic oscillator. This model does not totally represent the situation in a molecular laser. In particular it neglects rotation and vibration-vibration (V-V) collisions. Nonetheless, for reasons discussed in Appendix B, we believe it has some pertinence to cascades in diatomic molecules. As discussed in Sec. V, the small intensity restriction is not as severe in the cascade

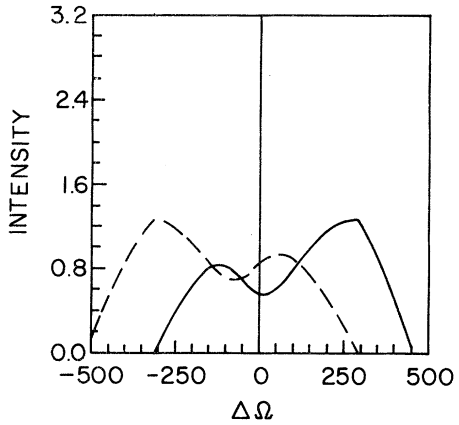

FIG. 11. Graph of three-level competitive transitions versus cavity detuning for the gas case with the two transitions detuned from each other by 50 MHz. Solid line and dashed lines correspond to 23 and 21 transitions of Fig. 1(b). Laser parameters are the same as in Fig. 7.

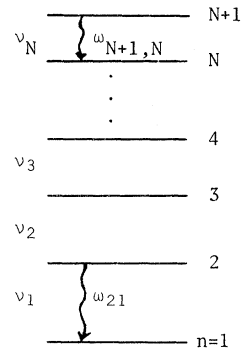

FIG. 12. Energy-level diagram for a multilevel cascade.

case as in the competitive case due to the partial cancellation of neglected higher-order terms. The relevant coefficients can be obtained by inspection from the simpler values in Sec. IV. Hence, in this section we give only the density-matrix and laser-intensity equations of motion, by way of defining the model quantitatively. Table III gives the coefficients for the homogeneously broadened medium. The Doppler and general cases are given by the same set of subscript substitutions from the corresponding three-level cases. The section closes with some numerical results.

We assume that only one cavity mode is resonant with any given transition of the cascade chain. This yields the electric dipole perturbation-energy matrix elements

$$\mathcal{V}_{n+k,n}=\begin{cases}-\frac{1}{2}\wp_{n+1,n}E_n(t)\exp[-i(\nu_n t+\phi_n)]U_n(z), & k=1\\ 0, & k\neq 1,\end{cases} \tag{56}$$

where n refers to the lower level of the transition. Here, the ν's are all unequal ($\nu_n\neq\nu_p$ for $n\neq p$). The equations of motion for the density matrix components are

$$\dot{\rho}_{nn}=\lambda_n-\gamma_n\rho_{nn}-\frac{i}{\hbar}\left(\sum_{k=n\pm1}V_{nk}\rho_{kn}+\text{c.c.}\right), \tag{57}$$

$$\dot{\rho}_{np}=-(i\omega_{np}+\gamma_{np})\rho_{np}-\frac{i}{\hbar}\left(\sum_{k=n\pm1}V_{nk}\rho_{kp}-\sum_{k=p\pm1}\rho_{nk}V_{kp}\right). \tag{58}$$

The first-order contribution to the polarization $\mathcal{P}_n(t)$ of Eq. (18) [or (20)] is given by three-level value (34) with the subscript substitutions $2\to n$, $3\to n+1$. The third-order contribution for $\mathcal{P}_1$ is given by the three-level case and that for $\mathcal{P}_N$ by the three-level value for $\mathcal{P}_2$ (36) with the subscript substitutions $1\to N-1$, $2\to N$, $3\to N+1$. The third-order contributions for $\mathcal{P}_n$, $1<n<N$ include effects

TABLE III. Summary of coefficients appearing in intensity and frequency Eqs. (59) and (60). These reduce to values in Table I for appropriate choices of n.

Coefficient	Physical interpretation
$\alpha_n=-\frac{1}{2}\frac{\nu_n}{Q_n}+F^{(1)}_{n+1,n}\mathfrak{L}_{n+1,n}(\omega_{n+1,n}-\nu_n)$	linear net gain
$\beta_n=\mathfrak{L}^2_{n+1,n}(\omega_{n+1,n}-\nu_n)F^{(3)}_{n+1,n}$	self-saturation
$F^{(1)}_{n+1,n}=\frac{1}{2}\left(\frac{\nu_n\wp^2_{n+1,n}}{\hbar\epsilon_0\gamma_{n+1,n}}\right)\bar{N}_{n+1,n}$	first-order factor
$F^{(3)}_{n+1,n}=\frac{3}{2}(\wp_{n+1,n}/2\hbar)^2\gamma^{-1}_{n+1,n}F^{(1)}_{n+1,n}\left(\frac{1}{\gamma_{n+1}}+\frac{1}{\gamma_n}\right)$	third-order factor
$\sigma_n=\left(\frac{\omega_{n+1,n}-\nu_n}{\gamma_{n+1}}\right)\mathfrak{L}_{n+1,n}(\omega_{n+1,n}-\nu_n)F^{(1)}_{n+1,n}$	linear pulling
$\rho_n=\left(\frac{\omega_{n+1,n}-\nu_n}{\gamma_{n+1}}\right)\mathfrak{L}^2_{n+1,n}(\omega_{n+1,n}-\nu_n)F^{(3)}_{n+1,n}$	self-pushing
$\vartheta_{n,n,n\pm1,n\pm1}=-\frac{1}{8}i\nu_n\frac{(\wp_{n+1,n}\wp_{n+1\pm1,n\pm1})^2\bar{N}_{n+1\pm1,n\pm1}}{\hbar^3\epsilon_0\gamma_n\gamma_{n+1\pm1,n\pm1}}\times\mathfrak{D}_{n+1,n}(\omega_{n+1,n}-\nu_n)\mathfrak{L}_{n+1\pm1,n\pm1}(\omega_{n+1\pm1,n\pm1}-\nu_{n\pm1})$	cross saturation population depletion part
$\vartheta_{n,n\pm1,n\pm1,n}=-\frac{1}{16}i\nu_n[(\wp_{n+1,n}\wp_{n+1\pm1,n\pm1})^2/\hbar^3\epsilon_0]\mathfrak{D}_{n+1,n}(\omega_{n+1,n}-\nu_n)\times\mathfrak{D}_{n+\binom{2}{1},n-\binom{0}{1}}(\omega_{n+\binom{2}{1},n-\binom{0}{1}}-\nu_n-\nu_{n\pm1})\times[\bar{N}_{n+1\pm1,n\pm1}\mathfrak{D}_{n+1\pm1,n\pm1}(\omega_{n+1\pm1,n\pm1}-\nu_{n\pm1})-\bar{N}_{n+1,n}\mathfrak{D}_{n+1,n}(\omega_{n+1,n}-\nu_n)]$	cross-saturation quadrupole part
$\tau_{nm}+i\theta_{nm}=\vartheta_{nnmm}+\vartheta_{nmmn}$	total cross-saturation coefficients

from interactions with modes $n+1$ and $n-1$, which are given by similar simple subscript substitutions. These observations lead to the mode-intensity equations of motion

$$\dot{I}_n = 2I_n(\alpha_n - \beta_n I_n - \theta_{n,n+1}I_{n+1} - \theta_{n,n-1}I_{n-1}), \quad (59)$$

$$\nu_n + \dot{\phi}_n = \Omega_n + \sigma_n - \rho_n I_n - \tau_{n,n+1}I_{n+1} - \tau_{n,n-1}I_{n-1}, \quad (60)$$

in which $\theta_{1,0} = \theta_{N,N+1} = \tau_{1,0} = \tau_{N,N+1} = 0$. The various coefficients are defined in Table III for the homogeneously broadened case.

To illustrate the formalism, we present intensity plots for two five-mode homogeneously broadened cascade cases. The intensities are again given in dimensionless units, and the different pairs of adjacent transitions are weakly coupled, typically with a coupling constant of 0.108. We find that for the laser parameters chosen and even with the maximum excitations of $\mathfrak{N}=1.2$, the third-order theory still yields quite acceptable results for the intensities of the cascade transitions. Figure 13 shows graphs of the mode intensities versus the cavity detuning for the five modes, the first mode oscillating with $\mathfrak{N}=1.2$ and the other modes each pumped just to the threshold level, i.e., at $\mathfrak{N}_n = 1.0$. For reference, the first mode oscillating alone is indicated by a dotted line. The mutual aid in cascading processes is again evident. Since we pump all the lower levels (other than the uppermost one) just to the threshold, the increase in the intensities due to the additional transitions is not strong. Supplementary runs show a slight increase in the intensity of the upper transition occurs whenever a new (lower) mode starts to oscillate. This effect was also observed (as expected) in the simpler three-level cases (see, e.g., Figs. 4 and 6). This is the normal case in a multilevel cascade laser like CO. As a trial computer run we obtained intensity plots with pumping to the lower levels, too, and found that the intensities increase substantially by addition of an extra mode. However, this generally does not occur in experimental cases. Typically, one is interested in extracting the most energy by pumping a single level. In our runs we also used slightly decreasing values for the electric dipole moments $\wp_{n+1,n}$ coming down the ladder, a choice corresponding to the case for anharmonic diatomic molecules. Solutions for three-, four-, and five-mode cases with equal $\wp$'s yielded intensities slightly smaller than the previous corresponding cases. In another trial run we filtered out the middle transition to see whether the cascading process would go through, but obviously it introduces a huge loss to the cascade chain and the upper two modes and the lower two lased as two independent pairs (Fig. 14). Yardley[11] mentions similar experimental results in which the absorption of transitions by atmospheric water vapor may break the chain of the cascade. He noted also that the use of a grating to select individual lines results in loss of intensity or even completely quenching the laser oscillation.

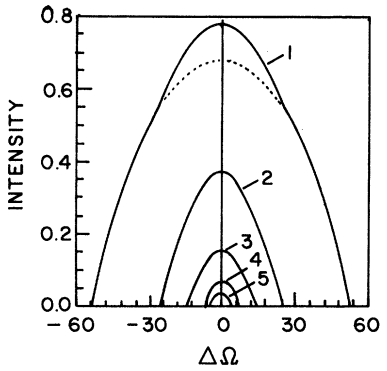

FIG. 13. Graphs of intensities of five modes oscillating together at $\mathfrak{N}_5 = 1.2$ and $\mathfrak{N}_4 = \mathfrak{N}_3 = \mathfrak{N}_2 = \mathfrak{N}_1 = 1.0$; $\gamma_6 = 20$, $\gamma_5 = 19$, $\gamma_4 = 17$, $\gamma_3 = 14$, $\gamma_2 = 12$, and $\gamma_1 = 9$ MHz; $\wp_{65} = 1.4$, $\wp_{54} = 1.35$, $\wp_{43} = 1.3$, $\wp_{32} = 1.25$, and $\wp_{21} = 1.2$.

APPENDIX A: POLARIZATION FOR ARBITRARY AMOUNT OF DOPPLER BROADENING

In this appendix we calculate the first- and third-order contributions to the polarization [Eq. (20)] of the laser medium for an arbitrary amount of Doppler broadening and for both two-mirror standing-wave and unidirectional ring-laser configurations. The technique employed relies on the per-

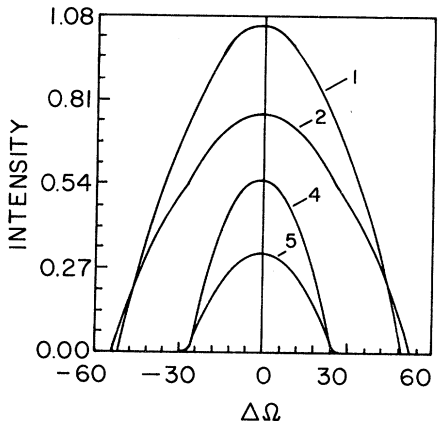

FIG. 14. Graphs of intensities of the five modes oscillating together at $\mathfrak{N}_5 = 1.2$, $\mathfrak{N}_4 = 1.0$, $\mathfrak{N}_3 = 0.2$, $\mathfrak{N}_2 = 1.2$, and $\mathfrak{N}_1 = 1.0$. Laser parameters used are same as in Fig. 13. As is seen in this graph, the third mode is not only filtered out, but it also breaks the cascade chain and the upper two modes and the lowest two oscillate as two independent pairs.

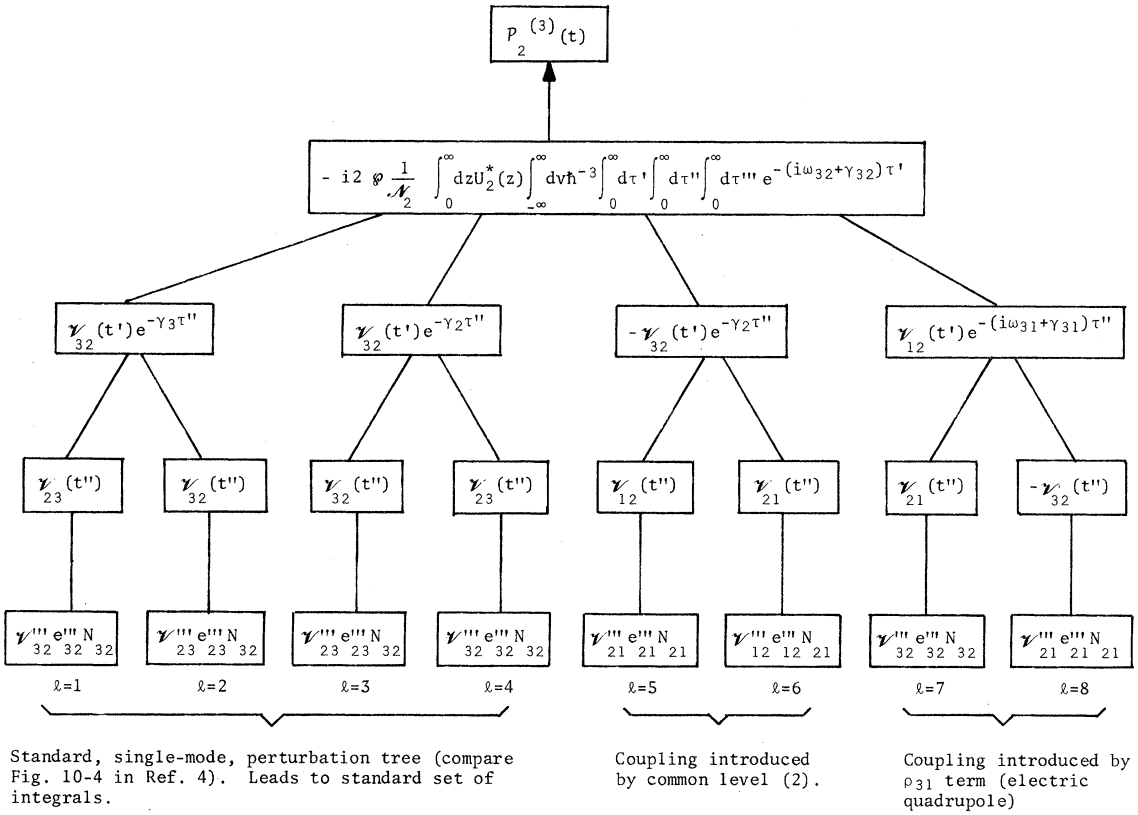

FIG. 15. Third-order perturbation tree for three-level system having density matrix equations of motion (11)–(16). The complex polarization $\mathcal{P}_n^{(3)}(t)$ is the third-order contribution to Eq. (20).

turbation tree discussed in Chap. 10 and Appendix D of Ref. 4. Inasmuch as this calculation is shorter and substantially more general than that of Sec. III, one might ask why both are included. We chose to give the simple case in Sec. III because of the probability that most individuals are not familiar with the perturbation tree, however powerful it is in treating problems of the present kind.

The first-order contribution to the polarization is identical to that for two-level systems (see Ref. 4) and deserves no further comment. The third-order contribution is represented by the tree in Fig. 15. Unlike the multimode treatment of two-level systems [see Eq. (D-3) of Ref. 4], it is generally necessary here to distinguish between wave numbers K_n in dealing with the Doppler shifts inasmuch as the K_n are associated with different transitions, leading to appreciable differences between the $K_n v$ factors. For this purpose, we expand the modal product

$$\Pi = U_n(z)U_\mu(z')U_\rho(z'')U_\sigma(z'''), \tag{A1}$$

where $z' = z - v\tau'$, $z'' = z - v\tau' - v\tau''$, $z''' = z - v\tau' - v\tau'' - v\tau'''$, and $U_n(z) = \sin(K_n z)$ explicitly. Using standard trigonometric identities and neglecting terms varying rapidly in space [like $\cos(2K_n z)$] and odd in v, we find

$$\begin{aligned}\Pi = \tfrac{1}{8}\{&\cos[(K_n - K_\mu - K_\rho + K_\sigma)z]\cos[K_\sigma v\tau''' - (K_\rho - K_\sigma)v\tau'' - (K_\mu + K_\rho - K_\sigma)v\tau'] \\ &+\cos[(K_n - K_\mu + K_\rho - K_\sigma)z]\cos[K_\sigma v\tau''' - (K_\rho - K_\sigma)v\tau'' + (K_\mu - K_\rho + K_\sigma)v\tau'] \\ &+\cos(K_n + K_\mu - K_\rho - K_\sigma)z\cos[K_\sigma v\tau''' + (K_\rho + K_\sigma)v\tau'' - (K_\mu - K_\rho - K_\sigma)v\tau']\}.\end{aligned} \tag{A2}$$

Taking the K_n's equal in the velocity cosines, we recover Eq. (D-3) of Ref. 4. For the tree limbs 5 and 6, we have the specialization $n = \mu = 2$, $\rho = \sigma = 1$. Defining the average wave number K and the constants c_n by

$$K=\tfrac{1}{2}(K_1+K_2),\quad K_n=c_nK, \tag{A3}$$

we have

$$\Pi(l=5,6)=\tfrac{1}{8}\{\cos[Kv(c_1\tau'''-c_2\tau')]+\cos[Kv(c_1\tau'''+c_2\tau')]+\cos[2(K_2-K_1)z]\cos[Kv(c_1\tau'''+2c_1\tau''+(2c_1-c_2)\tau')]\}. \tag{A4}$$

Here, the term with z dependence is assumed to vary sufficiently rapidly to cancel out in the spatial integration. Similar expressions result for the seventh and eighth limbs of the tree.

Writing the polarization contribution $\mathcal{P}_2^{(3)}$ from the tree, we have

$$\mathcal{P}_2^{(3)}=\tfrac{1}{16}\wp_{32}^2(\hbar^3Ku)^{-1}E_2\exp[-i(\nu_2t+\phi_2)]\left(\wp_{32}^2E_2^2\sum_{l=1}^{4}\sum_{w=1}^{3}T_{lw}+\wp_{21}^2E_1^2\sum_{l=5}^{8}\sum_{w=1}^{3}T_{lw}\right), \tag{A5}$$

where the complex third-order integral

$$T_{lw}=iN_{lw}K\pi^{-1/2}\int_{-\infty}^{\infty}dve^{-(v/w)^2}\int_0^{\infty}d\tau'\int_0^{\infty}d\tau''\int_0^{\infty}d\tau'''\exp\left(-\sum_{k=1}^{3}[v_{lk}+is_{wk}^{(l)}Kv\tau^{(k)}]\right), \tag{A6}$$

and the population inversion factors N_{lw} and constants $s_{wk}^{(l)}$ are defined in Table IV and the complex frequencies v_{lk} in Table V. The third-order complex coefficients are given by

$$\mathfrak{I}_{2222}=\tfrac{1}{32}\nu\wp_{32}^4(\hbar^3Ku\epsilon_0)^{-1}\sum_{l=1}^{4}\sum_{w=1}^{3}T_{lw}, \tag{A7}$$

$$\mathfrak{I}_{2211}=-\tfrac{1}{32}\nu(\wp_{32}\wp_{21})^2(\hbar^3Ku\epsilon_0)^{-1}\sum_{w=1}^{3}(T_{5w}+T_{6w}) \tag{A8}$$

$$\mathfrak{I}_{2112}=-\tfrac{1}{32}\nu(\wp_{32}\wp_{21})^2(\hbar^3Ku\epsilon_0)^{-1}\sum_{w=1}^{3}(-T_{7w}+T_{8w}). \tag{A9}$$

In the stationary system limit,

$$T_{lw}\xrightarrow[u\to 0]{}iKuN_{lw}/v_{l1}v_{l2}v_{l3},$$

and we recover the coefficients in Table I. In general, the T_{lw} are given by Eq. (D-9) of Ref. 4. In the Doppler limit, T_{5w} and T_{6w} are given by

$$T_{l1}=2i\pi^{1/2}\frac{N_{l1}}{v_{l2}}\frac{1}{c_1v_{l1}+c_2v_{l3}},\quad T_{l2},T_{l3}\to 0.$$

This gives

$$\mathfrak{I}_{2211}=-\tfrac{1}{16}i\nu\pi^{1/2}(\wp_{32}\wp_{21})^2(\hbar^3Ku\epsilon_0)^{-1}\bar{N}_{21}\gamma_2^{-1}\times[(c_1v_{51}+c_2v_{53})^{-1}+(c_1v_{61}+c_2v_{63})^{-1}]. \tag{A10}$$

For $c_1\simeq c_2\simeq 1$, this reduces to the value in Table II. The T_{71} term is multiplied by $N_{71}=0$. The other terms have negligible size in the Doppler limit. The T_{81} has nonzero value in the Doppler limit ($T_{82},T_{83}\simeq 0$), which for c_1 not too different from c_2 yields the value

$$\mathfrak{I}_{2112}=-\tfrac{1}{16}i\nu\pi^{1/2}(\wp_{32}\wp_{21})^2(\hbar^3Ku\epsilon_0)^{-1}\bar{N}_{21}\times\mathfrak{D}_{31}(\omega_{31}-\nu_1-\nu_2)(c_1v_{81}+c_2v_{83})^{-1}. \tag{A11}$$

This reduces to the value in Table II for $c_1=c_2=1$.

Inasmuch as we have taken $K_1\neq K_2$ in dropping terms with $\cos[2(K_1-K_2)z]$, one might ask how

TABLE IV. Definitions of factors $s_{wk}^{(l)}$ and population inversion factors N_{lw} appearing in third-order integrals (A6).

$s_{wk}^{(l)}$		$k=1$	$k=2$	$k=3$	N_{lw}
$l=1\to 4$	$w=1$	-1	0	1	$\bar{N}_{32}$
	2	1	0	1	$\bar{N}_{32}$
	3	1	2	1	$\bar{N}_{32}$
$l=5,6$	$w=1$	$-c_2$	0	c_1	$\bar{N}_{21}$
	2	c_2	0	c_1	$\bar{N}_{21}$
	3	$2c_1-c_2$	$2c_1$	c_1	0
$l=7$	$w=1$	$-(2c_1-c_2)$	c_2-c_1	c_2	0
	2	c_2	c_2-c_1	c_2	$\bar{N}_{32}$
	3	c_2	c_1+c_2	c_2	$\bar{N}_{32}$
$l=8$	$w=1$	$-c_2$	c_1-c_2	c_1	$\bar{N}_{21}$
	2	$2c_1-c_2$	c_1-c_2	c_1	0
	3	c_2	c_1+c_2	c_1	$\bar{N}_{21}$

TABLE V. Complex frequencies v_{lk} appearing in third-order integrals of (A6).

v_{lk}	$k=1$	$k=2$	$k=3$
$l=1$	$\gamma_{32}+i(\omega_{32}-\nu_2)$	γ_3	$\gamma_{32}+i(\omega_{32}-\nu_2)$
2	$\gamma_{32}+i(\omega_{32}-\nu_2)$	γ_3	$\gamma_{32}+i(\nu_2-\omega_{32})$
3	$\gamma_{32}+i(\omega_{32}-\nu_2)$	γ_2	$\gamma_{32}+i(\nu_2-\omega_{32})$
4	$\gamma_{32}+i(\omega_{32}-\nu_2)$	γ_2	$\gamma_{32}+i(\omega_{32}-\nu_2)$
5	$\gamma_{32}+i(\omega_{32}-\nu_2)$	γ_2	$\gamma_{21}+i(\omega_{21}-\nu_1)$
6	$\gamma_{32}+i(\omega_{32}-\nu_2)$	γ_2	$\gamma_{21}+i(\nu_1-\omega_{21})$
7	$\gamma_{32}+i(\omega_{32}-\nu_2)$	$\gamma_{31}+i(\omega_{31}-\nu_1-\nu_2)$	$\gamma_{32}+i(\omega_{32}-\nu_2)$
8	$\gamma_{32}+i(\omega_{32}-\nu_2)$	$\gamma_{31}+i(\omega_{31}-\nu_1-\nu_2)$	$\gamma_{21}+i(\omega_{21}-\nu_1)$

valid it is to simultaneously take $K_1 v \simeq K_2 v$. As given by (A10) or (A11), a substantial (e.g., 5%) difference between K_1 and K_2 (that is, between c_1 and c_2) leads to noticeable results. But only an appreciable change in the population inversions $N_{\alpha,\alpha-1}(z,t)$ over a distance $2\pi/2(K_1-K_2)$ can lead to a nonzero value of the $\cos[2(K_1-K_2)z]$ term after the z integration is performed. For example, for a 1-μm wavelength, if $N(z,t)$ changes by 50% or less over a centimeter, $\pi/(K_1-K_2)$ can equal a millimeter with essentially complete cancellation. This corresponds to $2\pi/K2(c_1-c_2)=0.1$ or $c_1-c_2=0.0005$, for which the approximation $c_1=c_2$ in (A10) or (A11) is excellent.

The running-wave ring-laser cases are also of interest. For these the field is given by

$$E(z,t)=\frac{1}{2}\sum_n E_n(t)\exp[-i(\nu_n t+\phi_n-K_n z)]+\text{c.c.}, \tag{A12}$$

where K_n can be taken negative to yield a wave propagating in the minus z direction. In the rotating-wave approximation, the perturbation energy $\upsilon_{n+1,n}$ reads

$$\upsilon_{n+1,n}=-\tfrac{1}{2}\wp_{n+1,n}E_n(t)\exp[-i(\nu_n t+\phi_n-K_n z)]. \tag{A13}$$

We consider two cases: unidirectional (both modes propagate along the z axis) and bidirectional (mode 2 propagates along z and mode 1 along minus z). The spatial mode product (A1) reduces in either case to

$$\Pi=\exp\{-iKv[(c_\mu+c_\rho+c_\sigma)\tau'+(c_\rho+c_\sigma)\tau''+c_\sigma\tau'''\]\}. \tag{A14}$$

From the perturbation tree, we write the various values of the c's as given in Table VI. The technique here is a simple example of the tabular method employed by O'Bryan and Sargent[12] and Hanson and Sargent[13]. The resulting T_{lw} integrals are also identified in the table from Table IV.

The complex saturation coefficients are then given by appropriate sums of the integrals in Table VI. Specifically, the complex self-saturation coefficient is

$$\vartheta_{2222}\equiv\rho_2+i\beta_2=\tfrac{1}{8}\nu\wp_{32}^4(\hbar^3 Ku\epsilon_0)^{-1}[T_{12}+T_{21}+T_{31}+T_{42}], \tag{A15}$$

The cross-depletion coefficient is (unidirectional)

$$\vartheta_{2211}=-\tfrac{1}{8}\nu(\wp_{32}\wp_{21})^2(\hbar^3 Ku\epsilon_0)^{-1}[T_{52}+T_{61}] \tag{A16}$$

and the quadrupole coefficient is (unidirectional)

$$\vartheta_{2112}=-\tfrac{1}{8}\nu(\wp_{32}\wp_{21})^2(\hbar^3 Ku\epsilon_0)^{-1}[-T_{73}+T_{83}], \tag{A17}$$

with similar expressions (easily summed from Table VI for the bidirectional cases. In particular, only the T_{l1} integrals survive in the Doppler limit, yielding

$$\vartheta_{2222}=\tfrac{1}{4}i\nu\pi^{1/2}\wp_{32}^4\overline{N}_{32}(\hbar^3 Ku\epsilon_0)^{-1}(\gamma_3^{-1}+\gamma_2^{-1})\times[c_1\upsilon_{21}+c_2\upsilon_{23}]^{-1}, \tag{A18}$$

$$\vartheta_{2211}=-\tfrac{1}{4}i\nu\pi^{1/2}(\wp_{32}\wp_{21})^2\overline{N}_{21}(\hbar^3 Ku\epsilon_0)^{-1}\gamma_2^{-1}\times[c_1\upsilon_{61}+c_2\upsilon_{63}]^{-1}, \tag{A19}$$

$$\vartheta_{2112}=0.$$

This leads to θ's half the size of the β's. On the other hand, the bidirectional case has a substantial quadrupole contribution due to the partial cancellation of Doppler shifts in the resonance de-

TABLE VI. Calculation of the third-order integrals (A6) for running-wave (ring) lasers. Both unidirectional (both modes travel in same direction) and bidirectional cases are considered. The c_n are determined from the perturbation tree in Fig. 15, with the energy matrix elements (A13) and the mode-factor product (A14).

l	c_μ	c_ρ	c_σ	$s_{w1}=c_\mu+c_\rho+c_\sigma$	$s_{w2}=c_\rho+c_\sigma$	$s_{w3}=c_\sigma$	T_{lw}	Case
1	c_2	$-c_2$	c_2	c_2	0	c_2	T_{12}	
2	c_2	c_2	$-c_2$	c_2	0	$-c_2$	T_{21}	either
3	c_2	c_2	$-c_2$	c_2	0	$-c_2$	T_{31}	
4	c_2	$-c_2$	c_2	c_2	0	c_2	T_{42}	
5	c_2	$-c_1$	c_1	c_2	0	c_1	T_{52}	
6	c_2	c_1	$-c_1$	c_2	0	$-c_1$	T_{61}	unidirectional
7	$-c_1$	c_1	c_2	c_2	c_1+c_2	c_2	T_{73}	
8	$-c_1$	c_2	c_1	c_2	c_1+c_2	c_1	T_{83}	
5	c_2	c_1	$-c_1$	c_2	0	$-c_1$	T_{51}	
6	c_2	$-c_1$	c_1	c_2	0	c_1	T_{62}	bidirectional
7	c_1	$-c_1$	c_2	c_2	c_2-c_1	c_2	T_{72}	
8	c_1	c_2	$-c_1$	c_2	c_2-c_1	$-c_1$	T_{81}	

nominator $1/[\gamma_{31}+i(\omega_{31}-\nu_1-\nu_2)]$, i.e., $\nu_1+K_1v+\nu_2-K_2v\sim\nu_1+\nu_2$ unless K_1 is very different from K_2. This is now a familiar type of cancellation due to the onset of two-photon spectroscopy.[14] Hence, the sum of the bidirectional cross-saturation coefficients has the Doppler limit value

$$\begin{aligned}\vartheta_{2211}+\vartheta_{2112}&\equiv\tau_{21}+i\,\theta_{21}\\&=-\tfrac{1}{4}i\nu\pi^{1/2}(\wp_{32}\wp_{21})^2\bar{N}_{21}(\hbar^3Ku\epsilon_0)^{-1}\\&\quad\times(\gamma_2^{-1}+v_{32}^{-1})[c_1v_{11}+c_2v_{33}]^{-1}.\end{aligned}\tag{A20}$$

As $\gamma_{31}\to\gamma_3$, this yields a θ_{21} approximately equal in magnitude but opposite in sign to β_2 of Eq. (A15). See Sec. V for a discussion of this somewhat anomalous low-saturation case. It is not clear to us how the case would be obtained experimentally. Moreover, in the multilevel cascade, with modes of alternating direction, the middle modes could, in fact, have more net gain than self-saturation leading to a breakdown of the third-order approach altogether. A similar cancellation of Doppler shifts occurs for the unidirectional competitive case, there leading to approximately equal β's and θ's and to standard mode-inhibition effects.

APPENDIX B: RELATIONSHIP TO DIATOMIC MOLECULES

Our model neglects numerous characteristics of diatomic molecules.[15] In particular, the molecules have a set of rotational levels (with magnetic sublevels) for each vibrational level, whereas we consider a single level alone. In support of this simplification, we note that typically only one rotational level per vibrational level is directly involved in laser action. Other rotational levels do interact indirectly through rapid collisions that repopulate the population distribution. To describe this phenomenon, we suppose that the Boltzmann distribution in the rotational levels corresponding to a single vibrational level is maintained in time through the collisions. As such the level lifetimes are not affected by the collisions, but the induced dipole moments dephase accordingly (the T_2 time is reduced, here represented by dipole decay constants like γ_{21}). Hence, we do not include any special factors in the atomic equations of motion to account for these processes.

V-V collisions lead to an effect that tends to pump an inversion.[11] Specifically, because the higher-lying levels are more closely spaced than the lower levels, the collision process

$$\mathrm{CO}(v-1)+\mathrm{CO}(1)\to\mathrm{CO}(v)+\mathrm{CO}(0)+\Delta E\tag{B1}$$

releases energy. The reverse process must absorb energy and is therefore less probable. Hence, V-V collisions tend to pump the molecules up higher in vibrational quantum number.

V-V rates decrease with increasing quantum number (as ΔE increases) and for sufficient high v ($v\sim30$)[16] radiative and vibration-translation (V-T) processes are the dominant factors in the relaxation rates. The V-V transition probabilities due to short-range forces decrease with lowering the temperature, but this is compensated by the long-range forces which increase the rate constants. Thus, V-V exchange in upper levels ($v>8$)[17] becomes the efficient process determining the level lifetimes (T_1) for the laser transitions. Hancock and Smith[17] and Jeffers and Kelley[18] discuss the V-V and V-T energy transfer rates. Once a small portion of CO molecules is vibrationally excited into the higher levels, the excited molecules relax mainly by the V-V energy exchange process, and since the lower levels have a larger decay rate, the ratios of population densities in the adjacent levels increases thereby allowing the lasing process to occur.[17] One might describe the time dependence of pumping and relaxation processes by writing the equation of motion for the population density ρ_{nn} of one of the levels (ignoring the small coherence terms) as

$$\begin{aligned}\dot{\rho}_{nn}=&-\sum_{k\neq n}W_{kn}\rho_{kk}\rho_{nn}+\sum_{k\neq n}W_{nk}\rho_{k+1,k+1}\rho_{n-1,n-1}\\&-(i/\hbar)[\text{the dipole interaction term}]_{nn},\end{aligned}\tag{B2}$$

where the W_{kn} are transfer rates. The kinetic terms also contain processes which take the molecule from n to $n+1$ level. These have been left out for reasons of simplicity. We suppose that, in steady-state cases, the decay "constant" γ_n and pump rate λ_n of (57) given by

$$\gamma_n\equiv\sum_{k\neq n}W_{kn}\rho_{kk}\tag{B3}$$

and

$$\lambda_n\equiv\sum_{k\neq n}W_{nk}\rho_{k+1,k+1}\rho_{n-1,n-1}\tag{B4}$$

are time and population independent.

A detailed study of dipole-moment function and vibration-rotation matrix elements for CO has been done by Young and Eachus[19] and others.[20-25] In our simplified model we use dipole-moment values that fit these models approximately. Caledonia and Center[26] developed a model for the steady-state vibrational distribution functions of anharmonic oscillators based on rate-equation type of solutions including the collisional exchange processes of V-V and V-T and the radiative decay rates for different species of gas present in the

system. Other theoretical models by Treanor, Rich, and Rehm[27] and Rich[28] are also based on the rate-equation approximation, and depict characteristics like small-signal gain versus vibrational quantum number v and vibrational populations versus v at different temperatures, pressures, and gas mixtures.

---

*This research supported in part by the Air Force Weapons Laboratory, Kirtland Air Force Base, New Mexico, 87117, and in part by Space and Missile Systems Organization, El Segundo, California.

[1]A. Javan, Phys. Rev. 107, 1579 (1957).
[2]H. Haken, R. Der Agobian, and M. Pauthier, Phys. Rev. 140, A437 (1965).
[3]W. E. Lamb, Jr., Phys. Rev. 134, A1429 (1964).
[4]M. Sargent III, M. O. Scully, and W. E. Lamb, Jr., *Laser Physics* (Addison-Wesley, Reading, Mass., 1974).
[5]M. S. Feld and A. Javan, Phys. Rev. 177, 540 (1969).
[6]B. J. Feldman and M. S. Feld, Phys. Rev. A 1, 1375 (1970).
[7]B. J. Feldman and M. S. Feld, Phys. Rev. A 5, 899 (1972).
[8]Th. Hänsch and P. Toschek, Z. Phys. 236, 213 (1970).
[9]I. M. Beterov and V. P. Chebotaev, in *Progress in Quantum Electronics*, edited by J. H. Sanders and S. Stenholm (Pergamon, Oxford, 1975), Pt. 1, Vol. 3.
[10]F. Najmabadi, Ph.D. dissertation (University of Arizona, 1974) (unpublished).
[11]J. T. Yardley, Appl. Opt. 10, 1760 (1971).
[12]C. L. O'Bryan and M. Sargent III, Phys. Rev. A 8, 3071 (1973).
[13]D. R. Hanson and M. Sargent III, Phys. Rev. A 9, 466 (1974).
[14]M. D. Levenson and N. Bloembergen, Phys. Rev. Lett. 32, 645 (1974); F. Biraben, B. Cagnac, and G. Grynberg, *ibid.* 32, 643 (1974); D. Pritchard, J. Apt, and T. W. Ducas, *ibid.* 32, 641 (1974); P. B. Kramer, S. R. Lundeen, B. O. Clark, and F. M. Pipkin, *ibid.* 32, 635 (1974); J. E. Bjorkholm and P. F. Liao, *ibid.* 33, 128 (1974).
[15]G. Herzberg, *Spectra of Diatomic Molecules* (Van Nostrand, New York, 1950), Vol. I.
[16]G. Hancock and J. W. M. Smith, Appl. Opt. 10, 1827 (1971).
[17]W. C. Eppers, Jr., R. M. Osgood, Jr., and P. R. Greason, IEEE J. Quantum Electron. 6, 4 (1970).
[18]W. Q. Jeffers and J. D. Kelley, J. Chem. Phys. 55, 4433 (1971).
[19]L. E. Young and W. J. Eachus, J. Chem. Phys. 44, 4195 (1966).
[20]H. S. Heaps and G. Herzberg, Z. Phys. 133, 48 (1952).
[21]R. C. Herman and K. E. Schuler, J. Chem. Phys. 22, 481 (1954).
[22]R. Herman and R. F. Wallis, J. Chem. Phys. 23, 637 (1955).
[23]R. Herman and R. J. Rubin, Astrophys. J. 121, 533 (1955).
[24]R. Herman, R. W. Rathery, and R. J. Rubin, J. Mol. Spectry. 2, 369 (1958).
[25]K. Cashion, J. Mol. Spectrosc. 10, 182 (1963).
[26]G. E. Caledonia and R. E. Center, J. Chem. Phys. 55, 552 (1971).
[27]C. E. Treanor, J. W. Rich, and R. G. Rehm, J. Chem. Phys. 48, 1798 (1968).
[28]J. W. Rich, J. Appl. Phys. 42, 2719 (1971).